


# Miniaturized full-metal bandpass filter and multiplexer using circular spiral resonator

Rui-Sen Chen<sup>1,2</sup> | Lei Zhu<sup>2</sup> | Sai-Wai Wong<sup>1</sup> | Jing-Yu Lin<sup>3</sup> | Yang Yang<sup>3</sup>  | Yin Li<sup>1</sup> | Yejun He<sup>1</sup>

<sup>1</sup>College of Electronics and Information Engineering, Shenzhen University, Shenzhen, China

<sup>2</sup>Department of Electrical and Computer Engineering, Faculty of Science and Technology, University of Macau, Macau SAR, China

<sup>3</sup>School of Electrical and Data Engineering, University of Technology Sydney, Ultimo, Australia

## Correspondence

Sai-Wai Wong, College of Electronics and Information Engineering, Shenzhen University, Shenzhen, China.  
Email: wongsaiwai@ieec.org

## Funding information

Natural Science Foundation of Guangdong Province, Grant/Award Number: 2018A030313481; Shenzhen Science and Technology Programs, Grant/Award Number: JCYJ20190808145411289; Shenzhen University Research Startup Project of New Staff, Grant/Award Number: 860-000002110311; Shenzhen Science and Technology Programs, Grant/Award Number: JCYJ20180305124543176; Guangdong Basic and Applied Basic Research Foundation, Grant/Award Number: 2019A1515111166

## Abstract

This article proposes a new class of miniaturized full-metal bandpass filters (BPFs) and multiplexers using circular spiral resonators (CSRs). The proposed metal CSR is supported on the metal cavity's wall, which serves as a short-end resonator. This CSR has obvious size reduction compared to traditional cavity resonators and owns low insertion loss, high power capacity and high selectivity. Then, three BPFs using two, three and four CSRs are designed and analysed. All the proposed filters have transmission zeroes (TZs) produced by the source-load coupling without introducing additional coupling structure. The proposed CSR is further used to design diplexer and quadruplexer. All the proposed filters have ultra-compact size, especially, the size of quadruplexer is only  $0.23\lambda_0 \times 0.081\lambda_0 \times 0.067\lambda_0$ . Finally, the fourth-order filter and quadruplexer are fabricated and measured, the good agreement between the measured results and the simulated results validates the proposed design concepts.

## 1 | INTRODUCTION

Wireless communication technologies have come a long way since the world's first wireless telephone conversation occurred in the late 19th century. As a critical component of communication systems, microwave filters are required to have miniaturized size, low power loss, high power capacity and high selectivity. Planar transmission line has been widely used to design filters with compact size [1–6], such as a microstrip line and substrate integrated waveguide (SIW). All of these filters have very compact size and are easy to design but suffer from high power loss and low power capacity. Cavity resonators, such as rectangular waveguide resonators [7, 8], cylindrical waveguide resonators [9, 10], coaxial cavity resonators [11, 12], dielectric-loaded cavity resonators [13, 14] have much higher unload

quality factor in comparison with planar resonators and own low power loss, large power capacity and sharp filtering selectivity. However, the cavity filters have a significant disadvantage in miniaturization design. Helical resonators have been used to design cavity filters with miniaturized sizes [15–18]. The helical structure has an apparent advantage over the miniaturization design comparing with the previously mentioned cavity filters. However, this approach is often found to be complex during the fabrication process because of its 3D structure.

Multiplexers are widely used to propagate RF signals into different channels in modern wireless communication systems. These multiplexers have required miniaturized size, low insertion loss and high power capacity. Conventional planar multiplexers [19, 20] and cavity-type multiplexers [7, 21–24] have been widely reported in over the last decade, but they

This is an open access article under the terms of the Creative Commons Attribution License, which permits use, distribution and reproduction in any medium, provided the original work is properly cited.

© 2021 The Authors. *IET Microwaves, Antennas & Propagation* published by John Wiley & Sons Ltd on behalf of The Institution of Engineering and Technology.

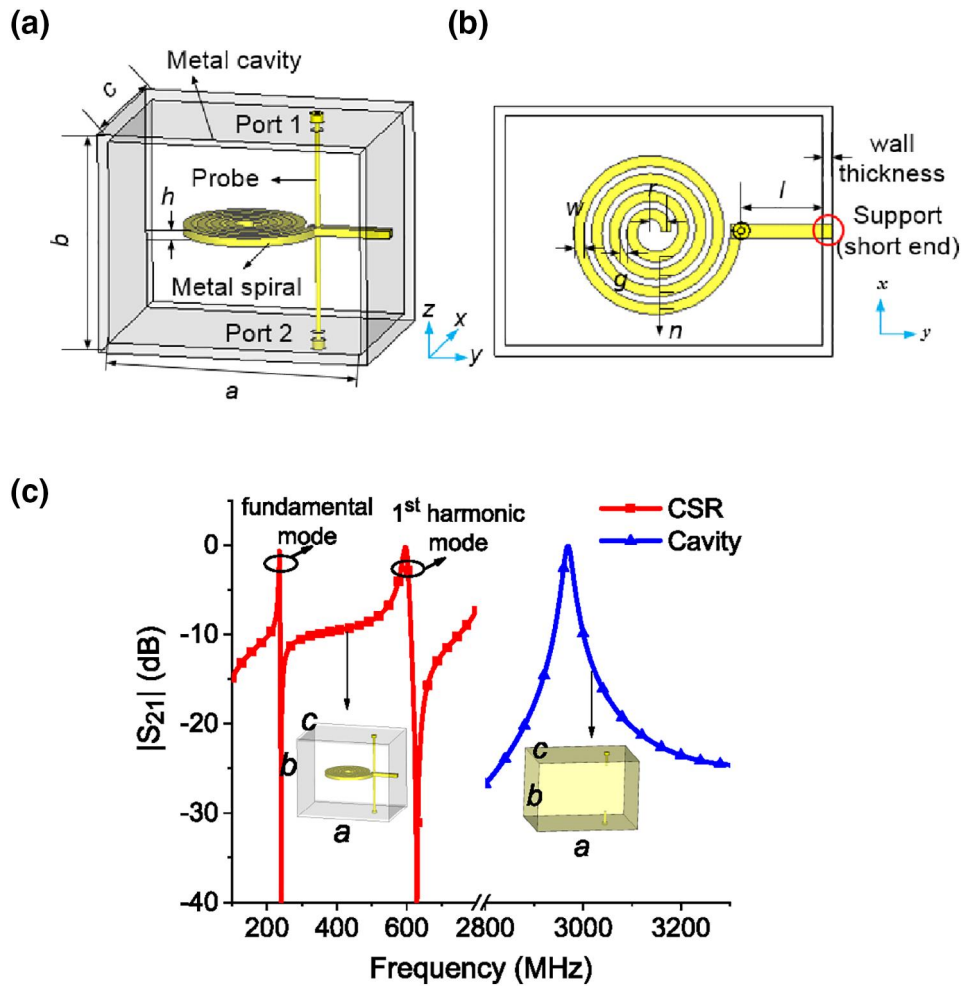


FIGURE 1 (a) Three-dimensional view of the proposed spiral resonator. (b) Top view. (c) Resonant frequencies of the traditional cavity and proposed spiral resonator

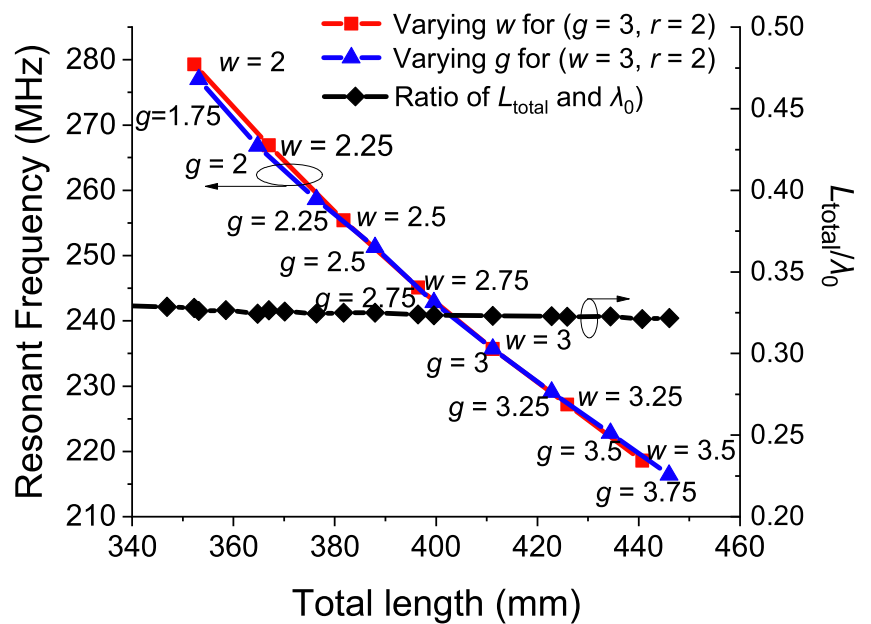
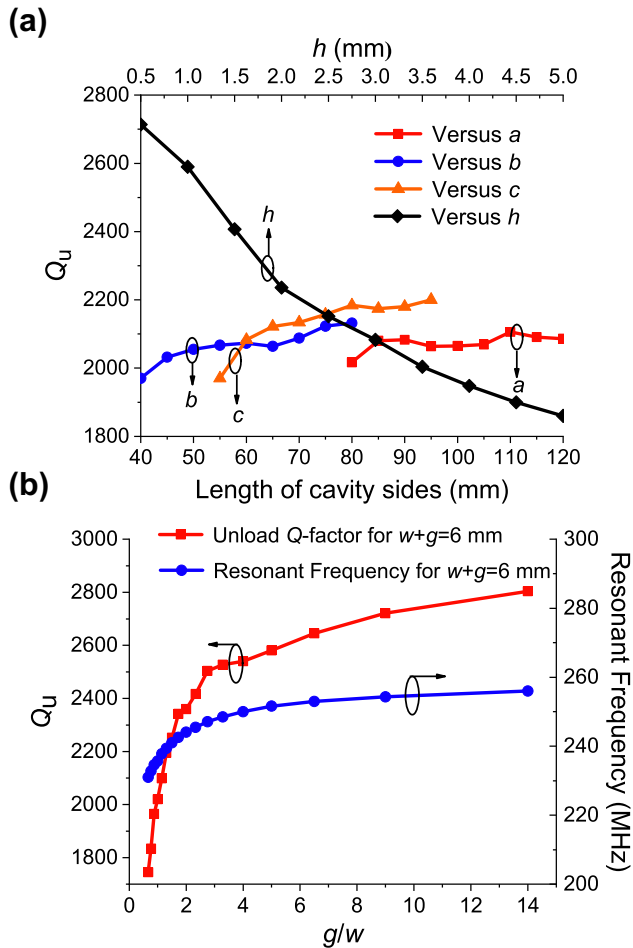


FIGURE 2 Frequency variation against  $L_{total}$  and variation of  $L_{total}/\lambda_0$  against  $L_{total}$

suffer from the similar problems as that explained in aforementioned filters, such as low power capacity in planar circuit and large circuit size in cavity circuit. Owing to the high demand of compact circuit size, the method of cavity multiplexers' miniaturization is in an imperious demand.



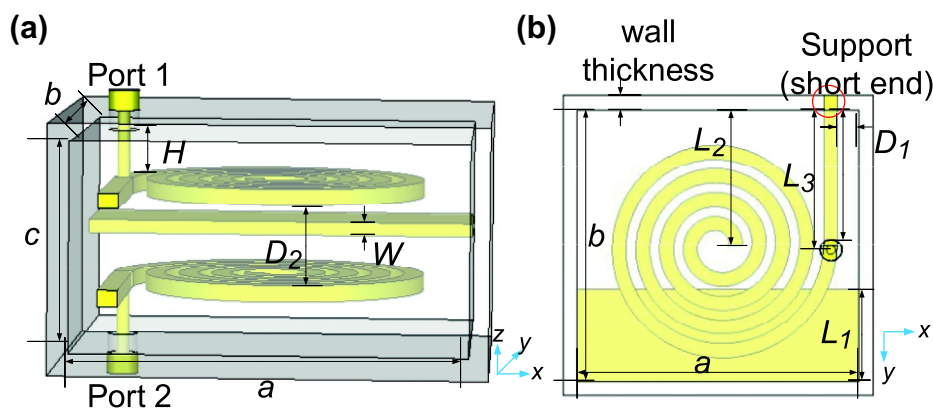
**FIGURE 3** (a) Unload Q-factor of the CSR versus the side lengths of the cavity ( $a$ ,  $b$  and  $c$ ) and thickness  $h$ ; (b) Unload Q-factor and resonant frequency versus ratio  $w/g$

The circular spiral resonator (CSR) embedded in a metal cavity is first proposed in [25], which demonstrates an obvious miniaturization property compared to the traditional metal cavity. However, the other performance of the CSR except for the miniaturized size was not analysed, such as the unloaded Q-factor, which is one of the main performances of a new resonator. In general, a smaller cavity size will result in a relatively lower unloaded Q-factor. Thus, it is necessary to discuss the unloaded Q-factor of the proposed spiral resonator. In our previous work [26], a dual-band filter based on the dual-mode CSR was presented. On the one hand, these two previous works were both second-order filters, which was an elementary design example of the proposed spiral resonator. It is necessary to show the feasibility in designing high-order filter based on the CSR. On the other hand, these two previous works focussed on the single-channel bandpass filter, it would be worthy to show the feasibility in designing multiplexing filters, such as the diplexer and the quadruplexer.

The novel CSR is further analysed in detail, including analysis of resonant frequency and unloaded Q-factor. Two high-order filters, that is, a third-order and a fourth-order using CSRs are further presented and designed except for the second-order filter. These filters are designed based on the coupling mechanism and coupling matrix. Good agreement is achieved between the theoretical response and simulation. In addition, a diplexer and a quadruplexer based on the second-order BPF are designed in Section 4, each channel has two TZs produced by the source-load coupling. The size of quadruplexer is only  $0.23\lambda_0 \times 0.081\lambda_0 \times 0.067\lambda_0$ , which is much compact than the published multiplexers. Finally, the fourth-order BPF and quadruplexer are fabricated and measured to validate the proposed design methods.

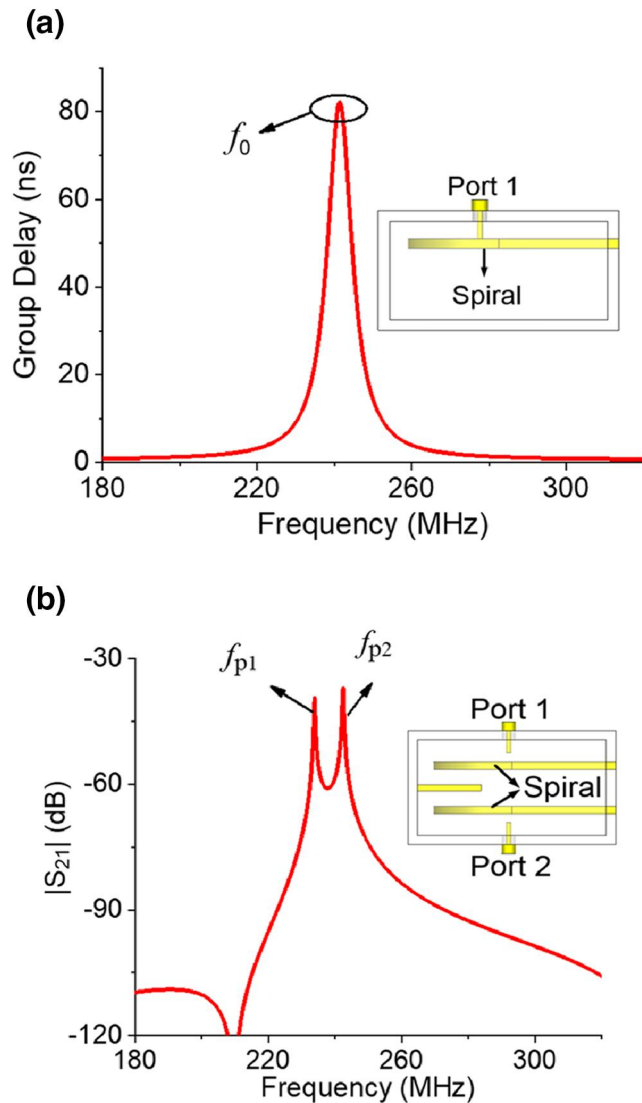
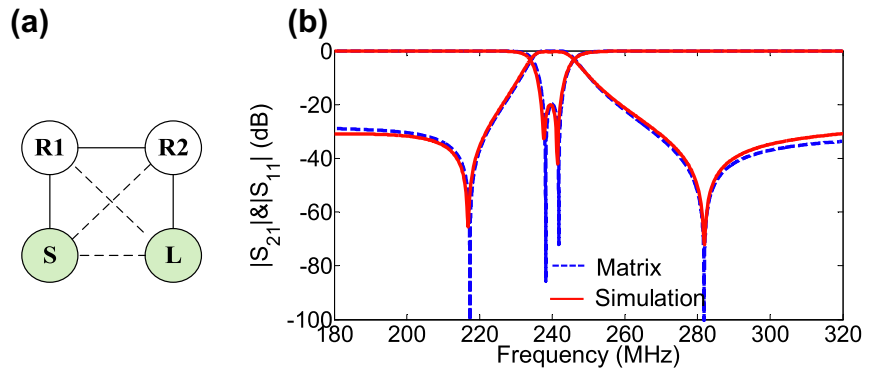
## 2 | ANALYSIS OF CIRCULAR SPIRAL RESONATOR IN A CAVITY

Figure 1a,b shows the configuration of proposed CSR with marked dimensions, which includes a metal circular spiral, a metal rectangular strip and a metal cavity. The dimensions of



**FIGURE 4** Second-order BPF: (a) Three-dimensional view and (b) Top view. Dimensions (Unit: mm, except  $n$ ):  $r = 2$ ,  $g = 2.1$ ,  $b = 2.5$ ,  $w = 3$ ,  $n = 4$ ,  $a = 60.3$ ,  $b = 58$ ,  $c = 32$ ,  $L_1 = 19.5$ ,  $L_2 = 29$ ,  $L_3 = 30$ ,  $D_1 = 4.6$ ,  $D_2 = 12.2$ ,  $H = 7.4$ ,  $W = 2$

**FIGURE 5** (a) Coupling mechanism and (b) Matrix response and simulated results of the second-order filter



**FIGURE 6** Extraction methods and simulation models: (a)  $Q_E$ ; (b)  $K$

the spiral are determined by the height ( $h$ ), width ( $w$ ), inner radius ( $r$ ), gap ( $g$ ) and the number ( $n$ ) of turns. The initial dimensions are given as  $a = 90$ ,  $b = 60$ ,  $c = 60$ ,  $l = 24$ ,  $h = 3$ ,  $w = 3$ ,  $r = 2$ ,  $g = 2.5$  and  $n = 4$  (unit: mm, except  $n$ ). Here, the total length of the CSR is represented as  $L_{total}$ . The rectangular

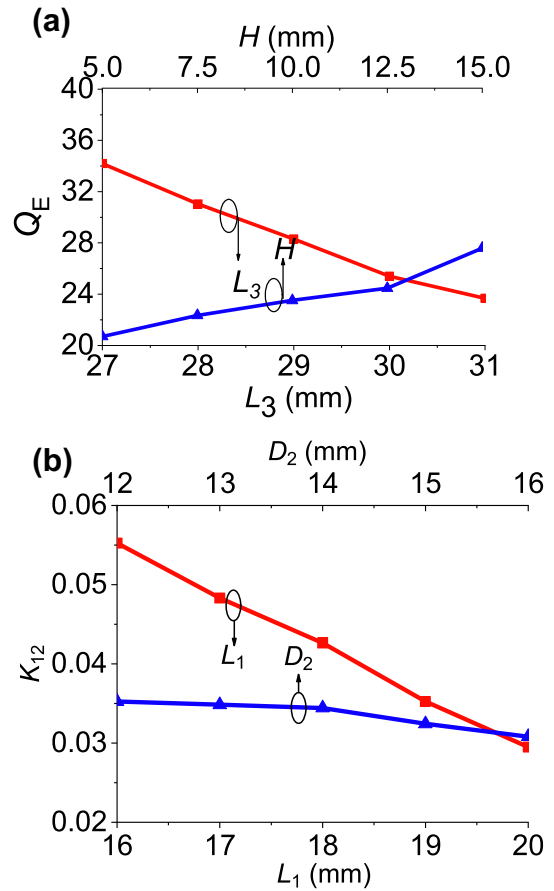


**FIGURE 7** Extracted results of second-order filter: (a)  $Q_E$ ; (b)  $K_{12}$

strip is a part of proposed CSR and is embedded into the cavity wall, which can support CSR on the cavity wall. Besides, it also contributes to the total length  $L_{total}$  of the CSR. Figure 1c shows the fundamental resonant frequencies of the traditional metal cavity and the proposed CSR using the same-size cavity. The former one resonates at 2970 MHz, while the latter one resonates at 250 MHz. The ratio between the two is about 11.8:1, which implies that the proposed CSR has obvious advantage of circuit miniaturization. Also, it has a TZ produced by the source-load coupling. The first parasitic mode  $f_{p1}$  is about  $2.56 \times f_0$ , which means that the proposed CSR has a high selectivity and a wide upper stopband-rejection.

Figure 2 plots the resonant frequency versus the total length  $L_{total}$ . The  $L_{total}$  is dependent on the dimensions of  $g$  and  $w$ . It shows that the resonant frequency of the fundamental mode  $f_0$  and decreases when the  $L_{total}$  increases due to the increasing of the equivalent parasitic inductance and capacitance. The total length of the resonator is about  $0.32\lambda_0$  (wavelength at  $f_0$ ).

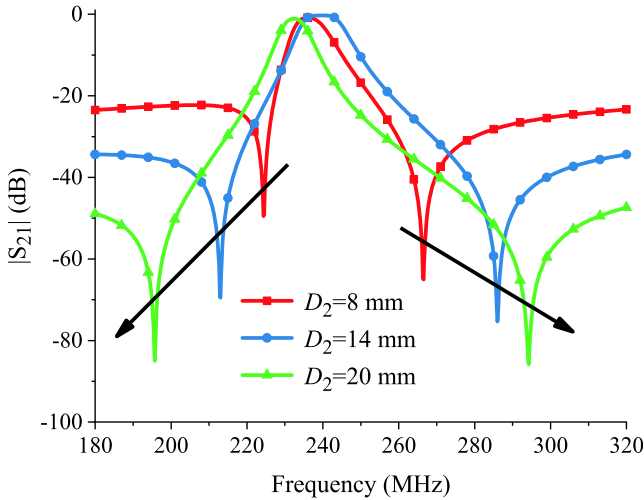


FIGURE 8 The position of the two TZs affected by the distance  $D_2$

Then, the unloaded Q-factor ( $Q_u$ ) of the proposed CSR is analysed.  $Q_u$  is one of the main performances of a resonator, which has not been analysed in the two precious works [25, 26]. The  $Q_u$  represents the inherent power loss of a resonator, which is related to the insertion loss of the filters. Figure 3a shows the  $Q_u$  influenced by the cavity size and the CSR thickness.

The increasing size of the cavity leads to a higher  $Q_u$ , which is contrary to the miniaturization design. The thickness of the CSR has an obvious effect on the  $Q_u$ , and a thinner CSR leads to a higher  $Q_u$ . When  $h = 0.5$  mm, the  $Q_u$  is about 2700. In fact, the  $Q_u$  can be sequentially increasing when choosing a thinner metal of CSR, but this will result in a weak rigidity for supporting the CSR on the cavity wall. Figure 3b depicts the  $Q_u$  and resonant frequency versus the ratio  $g/w$  under the condition of  $g + w = 6$  mm. We can see that the ratio  $g/w$  has a great effect on  $Q_u$  with the tendency that a high ratio  $g/w$  will result in a high  $Q_u$ , and the  $Q_u$  increases to 2800 when the ratio is set to 14. Although the traditional cavity resonators, such as the rectangular waveguide resonator, cylinder waveguide resonator and dielectric-loaded cavity resonator can achieve higher  $Q_u$  up to 5000 (or even higher), the proposed spiral resonator has obvious advantage over size reduction, which shows a good benefit and attractive characteristic in the design of RF/microwave circuits.

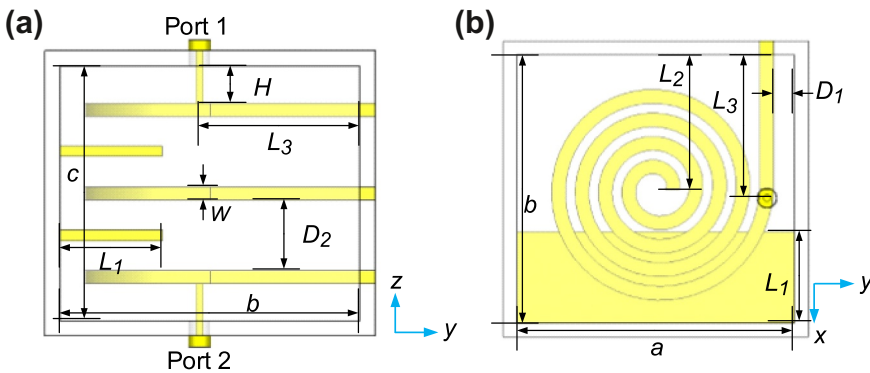


FIGURE 9 Third-order BPF (a) Side view and (b) Top view. Dimensions (unit: mm, except  $n$ ):  $r = 2, g = 2.1, h = 2.5, w = 3, n = 4, a = 60.3, b = 58, c = 49, L_1 = 19.8, L_2 = 29, L_3 = 31, D_1 = 4.6, D_2 = 13.65, H = 7.2, W = 2$

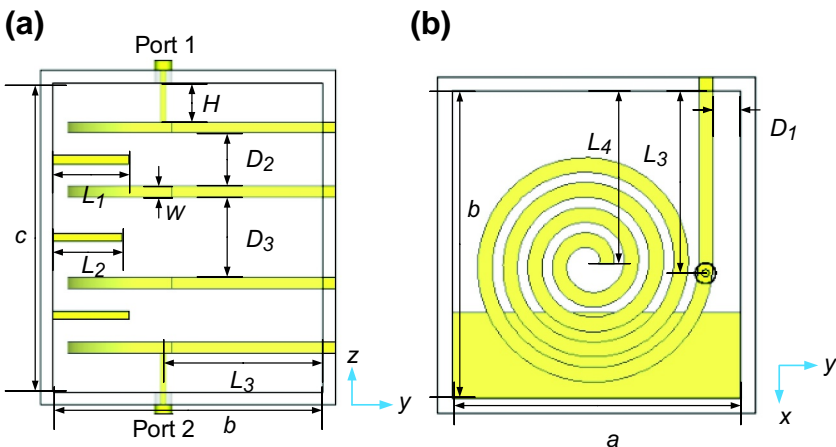
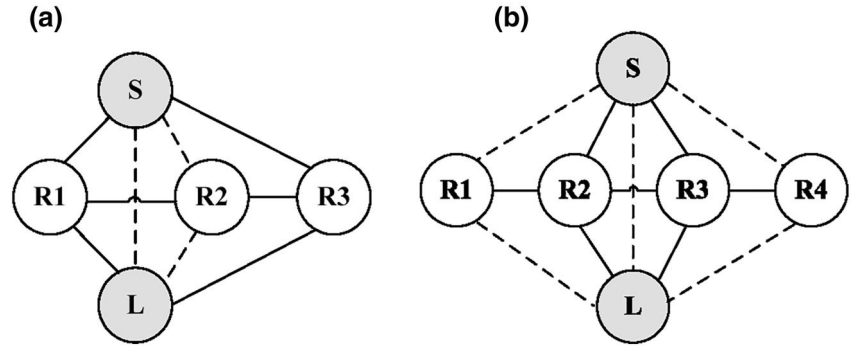


FIGURE 10 Fourth-order BPF (a) Side view; (b) Top view. Dimensions (unit: mm, except  $n$ ):  $r = 2, g = 2.1, h = 2.5, w = 3, n = 4, a = 69, b = 62.5, c = 71, L_1 = 17.5, L_2 = 16, L_3 = 37, L_4 = 35, D_1 = 5.6, D_2 = 12.25, D_3 = 18.5, H = 9, W = 2$

**FIGURE 11** Coupling mechanism: (a) Third-order and (b) Fourth-order



### 3 | FILTERS DESIGN BASED ON THE PROPOSED CIRCULAR SPIRAL RESONATOR

#### 3.1 | Second-order bandpass filter

As analysed in the previous section, the proposed CSR has a merit of size reduction and high unloaded Q-factor, which can be used to design filter with miniaturized size and low power loss. Then, a second-order filter using two CSRs sharing a single metal cavity is proposed, as shown in Figure 4a,b. The filter is fed by the coaxial cable with an extended probe.

The coupling topology is given as in Figure 5a, where the solid and dotted lines represent the positive coupling and negative coupling, respectively. The  $S$  and  $L$  represent the source and load, and  $R_i$  is the  $i$ -th resonator. The source-load coupling  $M_{SL}$  is produced by the coupling between the two probes.

As the existence of the indirect couplings, the coupling matrix is used as the design method. A two-order generalized Chebyshev filter with centre frequency, namely  $f_0$ , 240 MHz, fractional bandwidth (FBW) 5% and return loss 20 dB with two TZs at 217 and 282 MHz can be obtained by [27, 28]. The normalized  $[(n + 2) \times (n + 2)]$  coupling matrix  $M_{2nd}$  of the filter is given in Equation (1).

$$M_{2nd} = \begin{matrix} S \\ 1 \\ 2 \\ L \end{matrix} \begin{bmatrix} S & 1 & 2 & L \\ 0 & 0.9051 & -0.0785 & -0.0169 \\ 0.9051 & 0 & 0.9228 & 0 \\ 0 & 0.9228 & 0 & 0.9051 \\ -0.0169 & -0.0785 & 0.9051 & 0 \end{bmatrix} \quad (1)$$

The filtering response of the coupling matrix is shown in Figure 5b with blue-dotted lines. Owing to the existence of the unwanted diagonal cross-couplings  $M_{S2}$  and  $M_{L1}$  in matrix  $M_{2nd}$ , the response is asymmetric [29].

To realize the practical filter, the generalized coupling matrix is denormalized using the following formulas [30]:

$$Q_E = \frac{1}{\text{FBW} \cdot M_{S1}^2} K_{ij} = \text{FBW} \cdot M_{ij} \quad \text{FBW} = \frac{\text{BW}}{f_0} \quad (2)$$

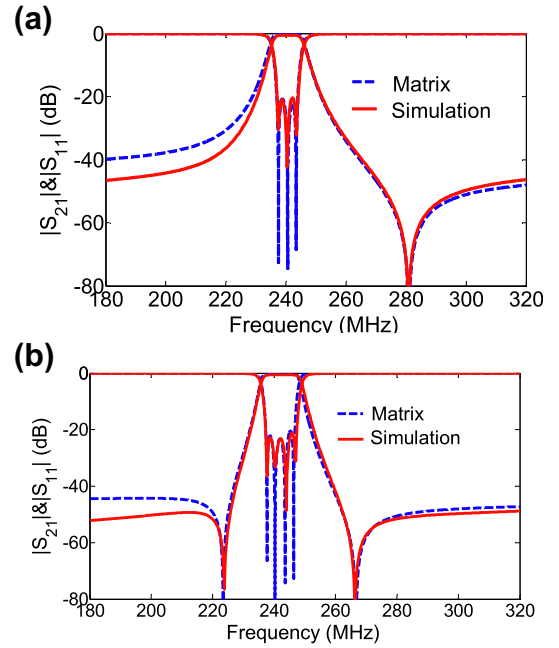


**FIGURE 12** Responses of coupling matrices and simulated results (a) Third-order filter; (b) Fourth-order filter

where  $Q_E$  and  $K_{ij}$  are the external quality factor and coupling coefficients of the practical filter, FBW is the fractional bandwidth, BW is the absolute bandwidth.  $M_{S1}$  and  $M_{ij}$  are the values in coupling matrix. Then, we get  $Q_E = 24.5$  and  $K_{12} = 0.046$ . The proposed filter is realized by implementing the normalized value in  $M_{2nd}$  to the practical design. The extraction formulas of the  $Q_E$  and coupling coefficient  $K$  are given as follows [31]:

$$Q_E = \frac{2\pi f_0 \cdot \tau_{S11}(f_0)}{4} \quad (3)$$

$$K = \frac{f_{p2}^2 - f_{p1}^2}{f_{p2}^2 + f_{p1}^2} \quad (4)$$

where  $\tau_{S11}(f_0)$  is the group delay of the  $|S_{11}|$  at the resonance  $f_0$ ,  $f_{p1}$  and  $f_{p2}$  are the resonance peaks of the two coupled resonators with weak excitation, as shown in Figure 6a,b with the simulation models.



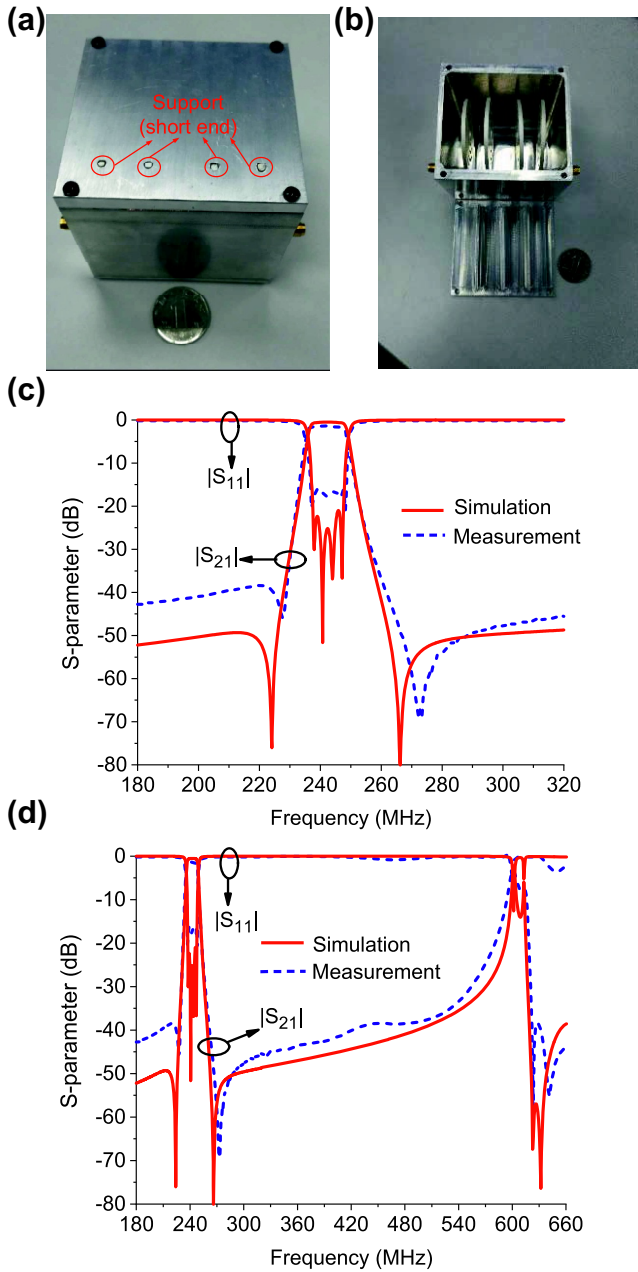


**FIGURE 13** Fourth-order BPF. (a) and (b) Photographs of the proposed fourth-order filter, (c) Comparison of measured and simulated results. (d) Comparison of measured and simulated results in a wide frequency range

The extracted results are plotted in Figure 7. The results show that the  $Q_E$  and  $K_{12}$  can be controlled by modifying the practical dimensions, which can cover the theoretical values. The initial practical dimensions of the filter are obtained by the previous analysis, and the desired performance can be finally achieved with simple optimization. The final simulated results are plotted in Figure 5b with red-solid line, and we observe that it matches very well with the matrix response. In simulation, the FBW is about 5% with the insertion loss 0.32 dB and return loss 20 dB.

In this filter, the TZs are produced by the source-load coupling  $M_{SL}$ , and a larger  $M_{SL}$  will make the TZs closer to passband. The source-load coupling is mainly controlled by the distance  $D_2$ . To discuss the controlling of the TZs, the TZs under the effect of varying  $D_2$  is shown in Figure 8. It can be seen that the TZs are closer to the passband with a smaller  $D_2$ , as a smaller  $D_2$  can produce a larger source-load coupling  $M_{SL}$ .

### 3.2 | High-order bandpass filter

The last subsection presents the design procedure of the BPF using the proposed CSR, where only the BPF with two order is presented. In this subsection, two high-order BPF, that is, third-order and fourth-order BPFs are further designed. The physical structures of them are shown in Figures 9 and 10, respectively. The spiral resonators are allocated in stack arrangement, which are in accordance with second-order BPF. The coupling mechanisms of the third-order and fourth-order BPFs are shown in Figure 11a,b, respectively.

Then, the coupling matrixes of the third-order BPF with  $f_0$  240 MHz, FBW 4.3%, return loss 20 dB and one TZ at 282 MHz, and the fourth-order BPF with  $f_0$  240 MHz, FBW 5.5%, return loss 20 dB and two TZs at 224 and 267 MHz, are obtained using the generalized Chebyshev theory [27, 28], and given in Equations (5) and (6), respectively. By using the extraction Equation (2), we obtain the theoretical  $Q$ -values and  $K$ -values, that is:

- (a) Third-order BPF:  $f_0 = 240$  MHz, FBW = 4.3%,  $Q_E = 27.2$ ,  $K_{12} = K_{23} = 0.0324$ .  
 (b) Fourth-order BPF:  $f_0 = 240$  MHz, FBW = 5.5%,  $Q_E = 22$ ,  $K_{12} = K_{34} = 0.037$ ,  $K_{23} = 0.0284$ .

**TABLE 1** Comparison with other reported filters

Ref.	Frequency (GHz)	Order	FBW	IL (dB)	Cavity Type	Size ( $\lambda_0 \times \lambda_0 \times \lambda_0$ )	TZ
[8]	5.5	3	58%	0.5	Rectangular waveguide	$0.81 \times 0.73 \times 0.44$	3
[14]	4.25	3	1.5%	1.3	Dielectric loaded	$0.37 \times 0.21 \times 0.27$	3
[16]	0.244	2	3.3%	0.18	Helical	$0.055 \times 0.043 \times 0.054$	1
[18]	0.43	4	3%	3.7	Helical	$0.107 \times 0.032 \times 0.042$	0
[25]	0.24	2	4.9%	0.4	Spiral	$0.049 \times 0.026 \times 0.047$	2
Proposed fourth order	0.242	4	5.3%	1.2	Spiral	$0.055 \times 0.05 \times 0.057$	2





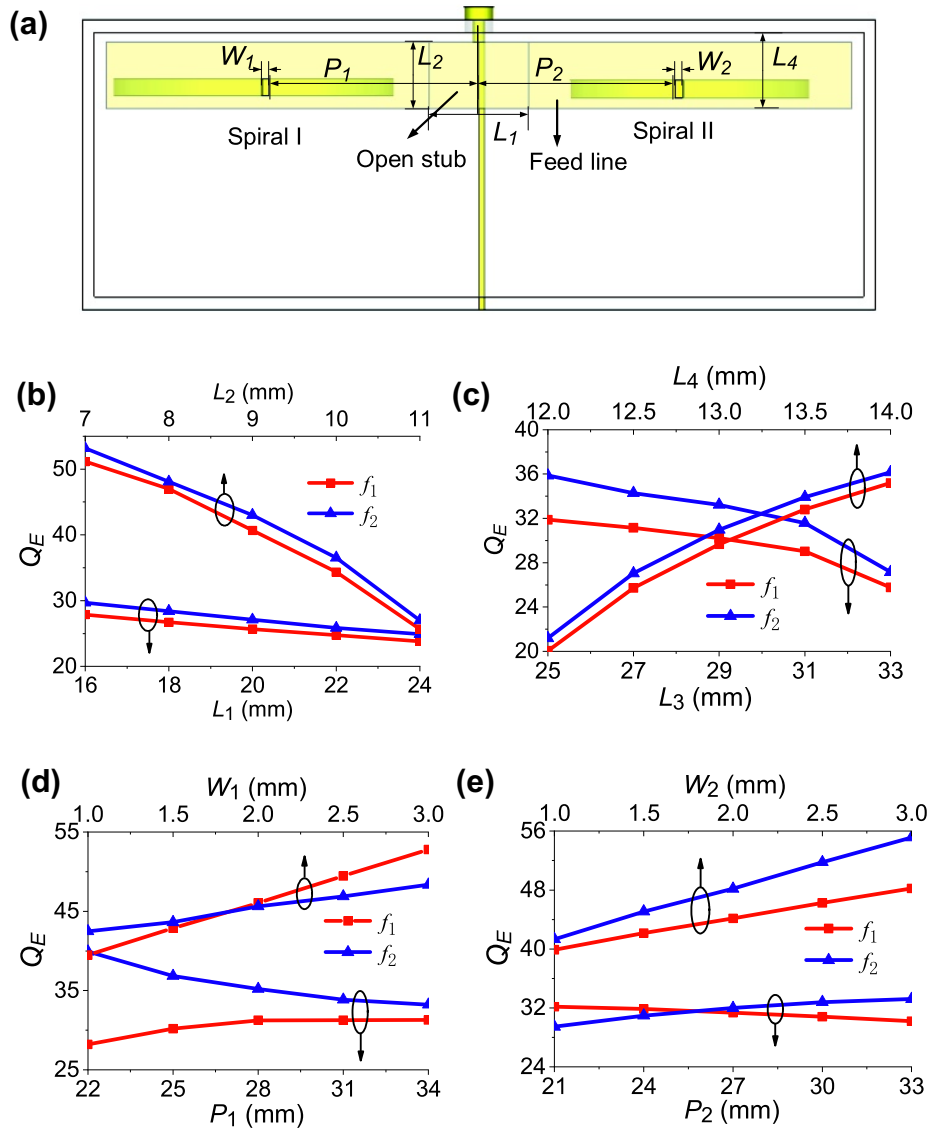


FIGURE 15 Extracted external  $Q$ -factor of the diplexer at common port (a) Simulated model; (b)–(e) extracted results

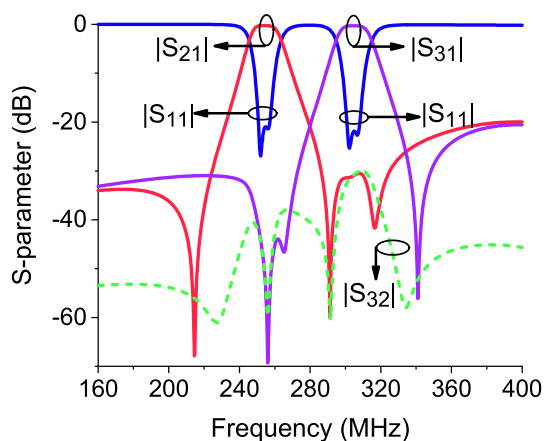


FIGURE 16 Simulated  $S$ -parameters of the proposed diplexer

and return loss (RL) are 1.2 and 15 dB, respectively, the centre frequency is 242 MHz with FBW 5.3%. The discrepancy between simulation and measurement is due to the discontinuity in the soldering between the probe and SMA, and between the probe and spiral, the fabrication roughness and assembly of the filter also affect the measured results. This filter also has a good upper-band rejection, as shown in Figure 13d, while the first spurious band occurred at 600 MHz, which is about 2.5 times the passband and keeps consistent with the spurious band of the CSR shown in Figure 1c. Although the helical filter in [16] has a lower insertion loss, it has a larger size than the spiral filter in [25] under the condition of same order.

The proposed BPFs are then compared with other reported filters, which is provided in Table 1. The comparison indicates that the proposed filters own the merits of miniaturized circuit size, low loss and high selectivity.

## 4 | DESIGN OF THE DIPLEXER AND QUADRUPLEXER

### 4.1 | Design of diplexer

The BPFs presented in Section 3 and the previous works [25, 26] are all single-channel filters. In this section, the proposed CSR is further used to design the miniaturized multi-channel filters, that is, multiplexers. Figure 14a,b shows the configuration of a second-order diplexer based on the second-order BPF presented in previous section. It includes two pairs of CSRs with different sizes, a feed line with an open stub, a metallic wall and a metal cavity surrounding them. The CSRs with different total length resonate at different frequencies, as analysed in Section 2, and produce different passbands at two outputs. The marked dimensions of the CSRs are given as  $r_i$ ,  $g_i$ ,  $w_i$ ,  $b_i$  and  $n_i$ , where  $i = 1, 2$ , which is corresponding to Spirals 1 and 2.

In this diplexer, the isolation between port 2 and port 3 is weak as the two pairs of spiral resonators are closed to each other. Thus, a metallic wall is put between the two pairs of CSRs to improve the isolation rather than separating them far away from the source. In fact, the isolation of traditional cavity diplexers is guaranteed by the metallic walls of the cavity resonators, which can naturally isolate the coupling between two different channels. However, for the proposed diplexer, all the spiral resonators of different channels share a same single metal cavity, the inter-channel couplings between different channels are inevitable. Thus, the metallic wall is needed to improve the isolation.

The common feedline connecting to the input is used to excite two separated pairs of CSRs and produce passbands at the two channels. The total coupling mechanism is given in Figure 14c, each channel can be seen as a second-order BPF shown in Figure 4a, which means that each passbands has two TZs to improve the selectivity of the passbands. It is noteworthy that the source-load coupling in each channel is achieved without introducing any additional coupling structure, it's naturally generated by coupling between the common feedline and the outputs' feeding probes.

For the diplexer, on one hand, the coupling coefficients of each filter is identical to the conventional BPFs. On the other hand, as the two filters sharing a common port, they are not completely symmetrical, which results in asymmetrical excited structures of the filters. Noticed that, the asymmetrical excited structures do not mean asymmetrical  $Q_E$  at the two ports of each filters. Thus, in the design of multiplexing filter, the achievement of equal  $Q_E$  with asymmetrical excited structures at the two ports and the adjustment of  $Q_E$  at the common port for the multiple channels are required to be analysed.

The  $Q_E$  at port 2 and port 3, and the  $K$ -values are similar to the BPFs presented in Section 3,  $H_1$  and  $H_2$  control the  $K$ -values, while the  $(H_3, S_2)$  and  $(H_4, S_3)$  control the  $Q_E$  of these two channels, respectively. The main difference is the  $Q_E$  at common port, for diplexer, the two channel filters share a same port, that is, port 1. The  $Q_E$  at the common port is then extracted and analysed. The extraction model is plotted in

Figure 15a and the extracted results are plotted in Figure 15b–c. The smaller  $L_1, L_2, L_3$  and larger  $L_4$  will obtain a lower  $Q_E$  for both channels. While  $(P_1, W_1)$  and  $(P_2, W_2)$  are related to channels 1 and 2, respectively, the increasing  $P_1$  enlarges the  $Q_E$  at channel 1 and decreases the  $Q_E$  at channel 2. The increasing  $W_1$  causes the  $Q_E$  to increase at both channels, and channel 1 has higher changing rate, as shown in Figure 15d. The same analysis is suitable for the extracted  $Q_E$  versus  $P_2$ , and  $W_2$  shown in Figure 15e.

Then, a diplexer with centre frequency of 255 MHz, TZs at 215 MHz, 291 MHz for channel 1, and centre frequency of 305 MHz, TZs at 265 and 341 MHz for channel 2, is designed. Both channel filters are designed with 5% FBW and 20 dB return loss. As each channel is seen as a second-order filter, thus, the synthesis method of diplexer is similar to the filter. The theoretical  $Q$ -values and  $K$ -values can be obtained from the given matrixes, just like the bandpass filters designed in the Section 3. While the practical  $Q$ -values and  $K$ -values of each channel can be extracted using the method shown in Figures 6, 7 and 15. By matching the practical  $Q$ -values and  $K$ -values to theoretical values, we obtain the initial filters' dimensions. Following some optimization, the desired performances are achieved. The simulated S-parameters of the diplexer are shown in Figure 16. Channel one works at 255 MHz with insertion loss 0.28 dB and return loss 21 dB, while channel 2 works at 305 MHz with insertion loss 0.3 dB and return loss

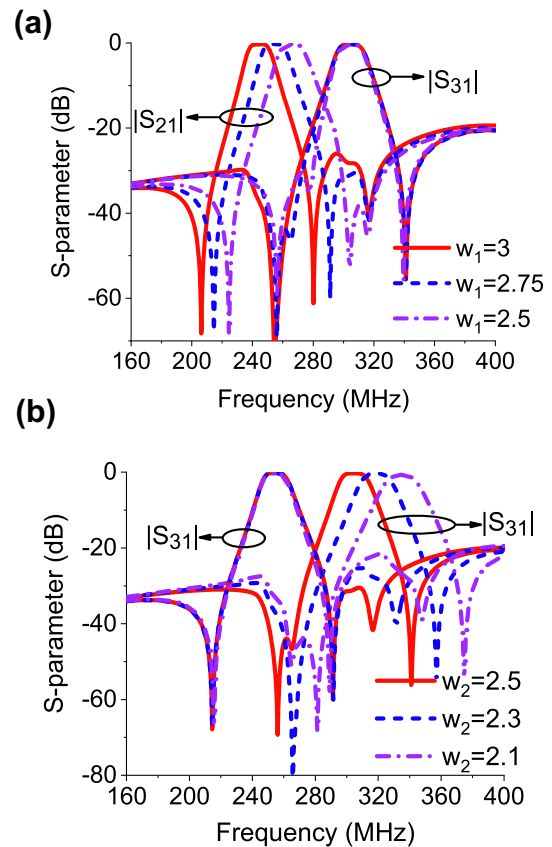


**FIGURE 17** Individual frequency-tuning of the diplexer (a) Channel 1; (b) Channel 2

22 dB. Both channels have one TZ at each side of the pass-band. Besides, the isolation between channels 1 and 2 is better than 30 dB.

As analysed in Section 2, the resonant frequency of the spiral resonator can be designed by modifying its total length. For the diplexer/multiplexer, we expect that the working frequencies of the different channels can be individually designed without affecting other channels. As shown in Figure 17, the working frequency of each channel can be modified by

changing the corresponding total length, while the frequency of other channel remains unchanged.

## 4.2 | Design of quadruplexer

Based on the previous design of diplexer, a second-order quadruplexer using four pairs of CSRs is presented and analysed. Figure 18a,b shows the configuration and of the

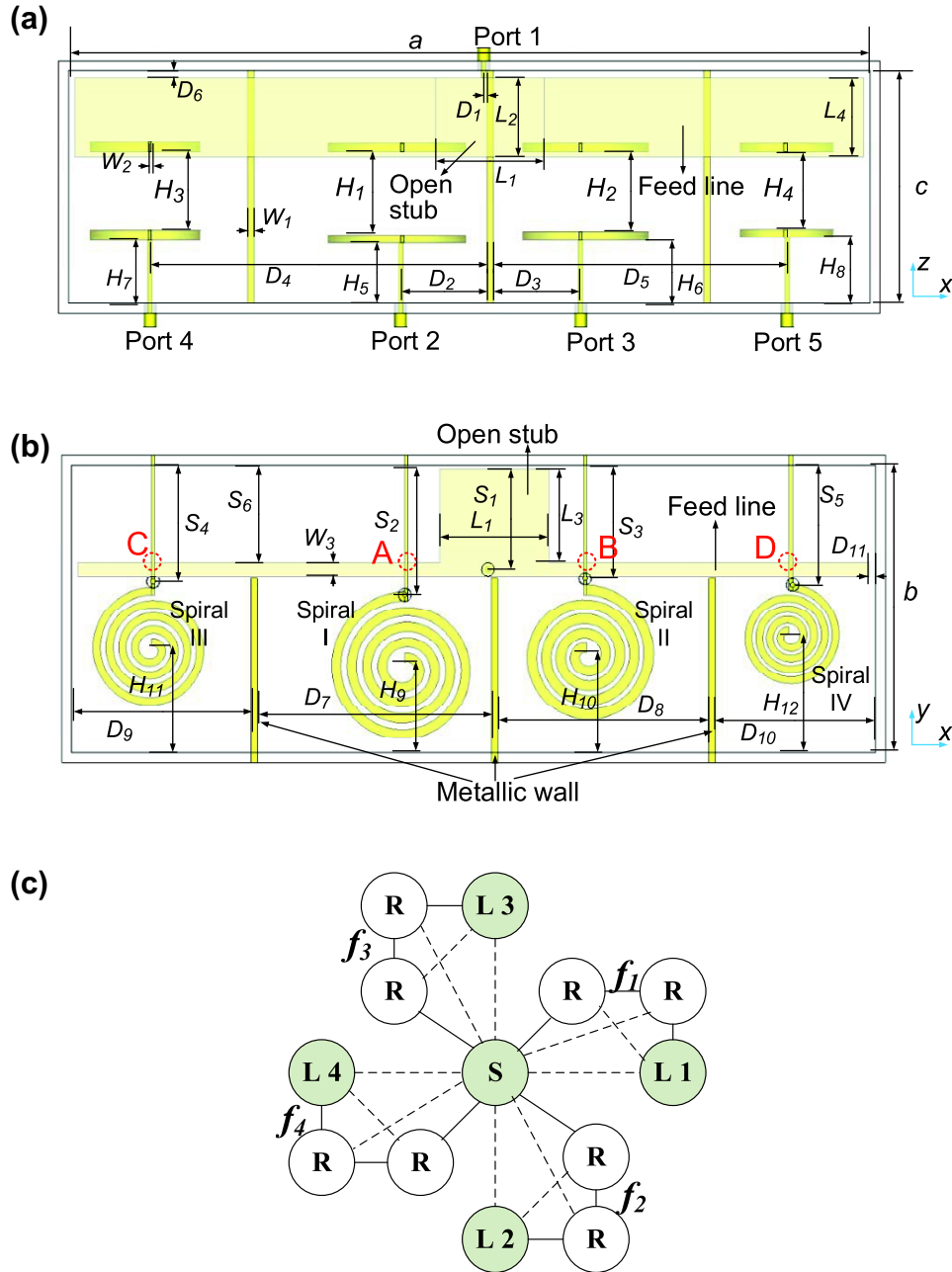
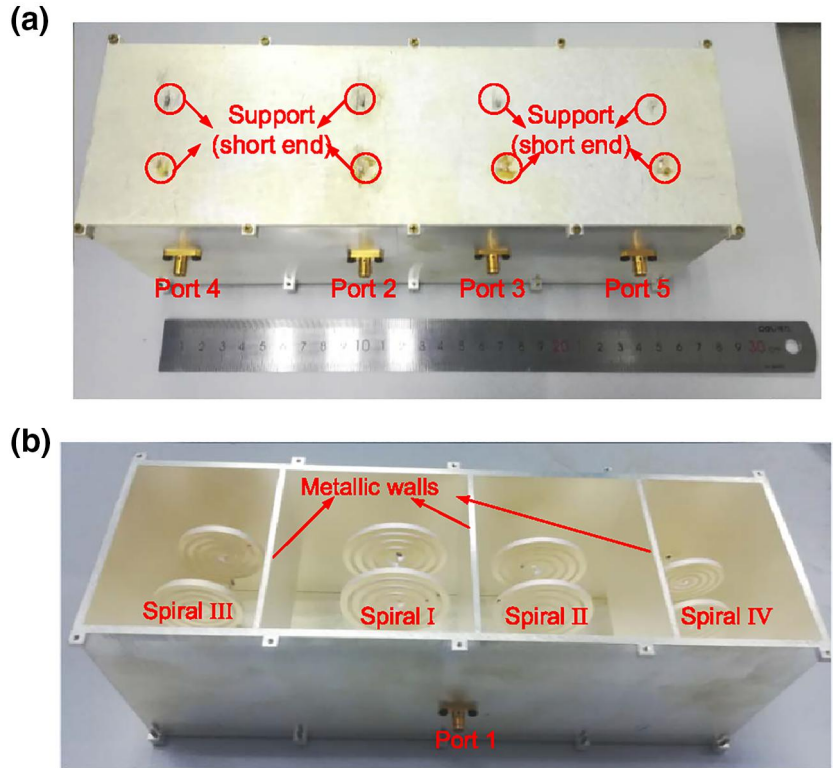


**FIGURE 18** (a) 3D view, (b) Top view and (c) Coupling mechanism of the proposed second-order quadruplexer. (A, B, C and D) Connections of feed line and CSRs). Dimensions (unit: mm, except  $n_1$ ,  $n_2$ ,  $n_3$ , and  $n_4$ ):  $r_1 = 2$ ,  $g_1 = 2$ ,  $h_1 = 2.5$ ,  $w_1 = 2.8$ ,  $n_1 = 4$ ,  $r_2 = 1$ ,  $g_2 = 1.5$ ,  $h_2 = 2.5$ ,  $w_2 = 3$ ,  $n_2 = 4$ ,  $r_3 = 1$ ,  $g_3 = 1.7$ ,  $h_3 = 3$ ,  $w_3 = 2.5$ ,  $n_3 = 4$ ,  $r_4 = 0.8$ ,  $g_4 = 1.2$ ,  $h_4 = 2.5$ ,  $w_4 = 2.15$ ,  $n_4 = 4$ ,  $a = 251$ ,  $b = 89$ ,  $c = 74$ ,  $L_1 = 34$ ,  $L_2 = 25$ ,  $L_3 = 29$ ,  $L_4 = 25$ ,  $D_1 = 1$ ,  $D_2 = 27$ ,  $D_3 = 27.3$ ,  $D_4 = 105.5$ ,  $D_5 = 92$ ,  $D_6 = 3$ ,  $D_7 = 73$ ,  $D_8 = 66$ ,  $D_9 = 56$ ,  $D_{10} = 50$ ,  $D_{11} = 1$ ,  $H_1 = 26.4$ ,  $H_2 = 25.3$ ,  $H_3 = 24.8$ ,  $H_4 = 24.5$ ,  $H_5 = 19.3$ ,  $H_6 = 20.4$ ,  $H_7 = 20.4$ ,  $H_8 = 21.2$ ,  $H_9 = 28$ ,  $H_{10} = 31$ ,  $H_{11} = 33$ ,  $H_{12} = 36.8$ ,  $S_1 = 32$ ,  $S_2 = 40$ ,  $S_3 = 35$ ,  $S_4 = 36$ ,  $S_5 = 37$ ,  $S_6 = 30$ ,  $W_1 = 2$ ,  $W_2 = 1$ ,  $W_3 = 4$

**FIGURE 19** Photograph of the quadruplexer  
(a) Full view and (b) Inside view



proposed quadruplexer with marked dimensions. Each of the two pairs of CSRs is placed at the right and left sides of the input terminal. This purposed arrangement is chosen due to the fact that if four pairs of CSRs are all placed in one side, the channels far from the input terminal will have very weak excitation, resulting in poor in-band performance. Each metallic wall is placed between adjacent pairs of CSRs to enhance the isolation. As discussed previously, each channel can be seen as a second-order BPF presented in Section 2. Thus, the coupling mechanism is given in Figure 18c, the source-load coupling in each channel will produce a pair of out-of-band TZs. The marked dimensions of the CSRs are given as  $r_i$ ,  $g_i$ ,  $w_i$ ,  $h_i$  and  $n_i$ , where  $i = 1, 2, 3, 4$ , which is corresponding to Spirals 1, 2, 3 and 4, as shown in Figure 18b. The definitions of  $r$ ,  $g$ ,  $w$ ,  $h$  and  $n$  are given in Section 2, other marked dimensions of the circuit are shown in Figure 18a,b. Similar to the diplexer, the resonant frequencies of the four passbands can be individually designed by modifying the respective total lengths  $L_{total}$ . The design procedure of the quadruplexer is similar to the diplexer presented in the last subsection, the coupling coefficients,  $Q_E$  in common port (port 1), and  $Q_E$  belong to the outputs of four channels and can be modified to the desired values to achieve the desired performance.

Finally, the quadruplexer is fabricated and measured. The photographs are shown in Figure 19a,b. The comparison between measurement and simulation are given in Figure 20a,b with dashed line and solid line, respectively. According to simulated results, we see that the working frequencies of the four channels are 274 MHz, 312 MHz, 362 MHz and

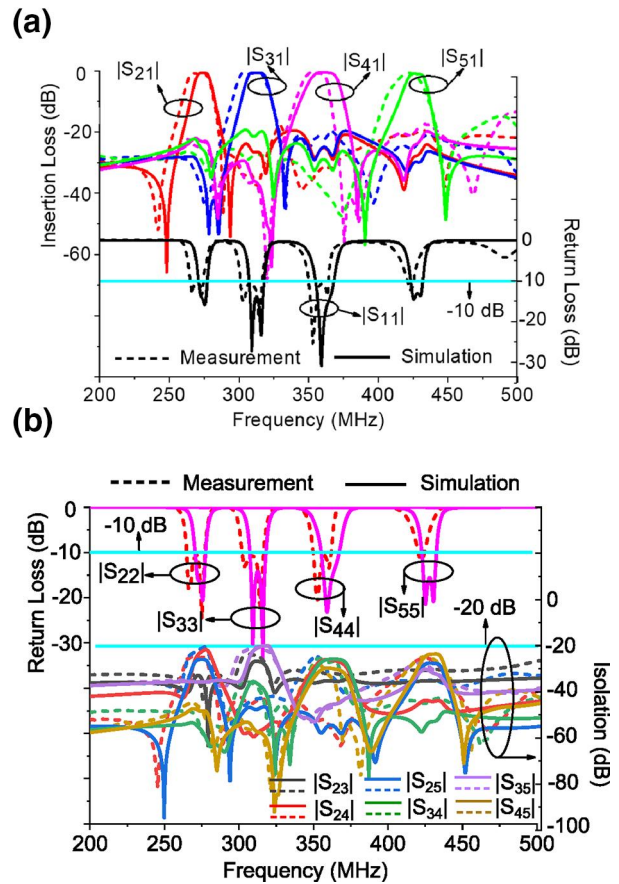


**FIGURE 20** Simulated and measurement of the quadruplexer.  
(a) Insertion loss and return loss (common port); (b) Return loss (outputs) and isolation

**TABLE 2** Comparison with other reported multiplexers

Ref.	Channel $\times$ Order	Frequency (GHz)	IL (dB)	Cavity Type	Size ( $\lambda_0 \times \lambda_0 \times \lambda_0$ )	TZ of Each Channel
[7]	3 $\times$ 2	2.87/3.06/3.23	0.6/1.0/1.0	Rectangular waveguide	2.21 $\times$ 1.42 $\times$ 1.04	0
[21]	3 $\times$ 4	4.375/5.125/5.875	0.67/0.9/0.93	Ridge waveguide	3.58 $\times$ 0.69 $\times$ 0.7	0
[22]	4 $\times$ 4	9.895/9.965/10.035/10.105	1.8/1.6/1.9/1.5	Rectangular waveguide	6.6 $\times$ 6.6 $\times$ 0.33	0
[23]	2 $\times$ 5	2.512/2.67	0.6/0.6	Coaxial Cavity	0.79 $\times$ 0.49 $\times$ 0.21	1
Proposed diplexer	2 $\times$ 2	0.245/0.299	0.28/0.3 Simu.	Spiral Cavity	0.1 $\times$ 0.077 $\times$ 0.035	2
Proposed quadruplexer	4 $\times$ 2	0.27/0.378/0.355/0.421	1.0/0.9/0.5/0.8	Spiral Cavity	0.23 $\times$ 0.081 $\times$ 0.067	2

428 MHz, respectively. The simulated FBW of them is 3.9%, 4.8%, 5.2%, and 3.5%, respectively. The insertion losses are 0.63 dB, 0.68 dB, 0.43 dB, and 1.0 dB, respectively, while the return losses in the common port (port 1) are 14.7 dB, 13.8 dB, 14.3 dB, and 13 dB, respectively. The return losses of outputs are higher than 14 dB. The simulated isolation is  $|S_{23}| = -27$  dB,  $|S_{24}| = -22$  dB,  $|S_{25}| = -26$  dB,  $|S_{34}| = -26$  dB,  $|S_{35}| = -20$  dB,  $|S_{45}| = -24$  dB. The measured working frequencies are 270 MHz, 307 MHz, 355 MHz and 421 MHz with insertion losses 1.0 dB, 0.9 dB, 0.5 dB, 0.8 dB, respectively. The measured FBW of them is 4.7%, 5.5%, 4.8%, and 4.1%, respectively. All the measured return losses are better than 10 dB. The discrepancy between simulation and measurement is due to the fabrication and measurement errors. Both the simulation and measurement show that isolations are higher than 20 dB. The sharp-skirt roll-off rates in both sides of each passband are achieved.

The comparison with other reported multiplexers is shown in Table 2, which demonstrates that the proposed multiplexers have the merits of ultra-miniaturized size converted to the same-order and same-channel multiplexers, and also owns low loss and high selectivity.

## 5 | CONCLUSION

The miniaturized cavity circuits using CSRs in a single metal cavity are demonstrated. The proposed CSR obtains an obvious size reduction compared to the traditional metal cavity. Then, three BPFs with TZs are analysed and designed. The filters have miniaturized circuit sizes and own high in-band performance. Meanwhile, a diplexer and a quadruplexer using two groups and four groups of second-order BPFs are presented, respectively. Each channel has two TZs to improve the selectivity and nearby stopband rejection. All of them have miniaturized circuit sizes. Finally, the fourth-order BPF and the quadruplexer are fabricated and measured, and the measured results have a good agreement with the simulated results.

## ACKNOWLEDGEMENTS

This work was supported in part by the National Natural Science Foundation of China under grant 62071306, in part by the Shenzhen Science and Technology Program under grant JCYJ20180305124543176, JCYJ20190728151457763, in part

by the Natural Science Foundation of Guangdong Province under grant 2018A030313481, and in part by Shenzhen University Research Startup Project of New Staff under grant 860-000002110311.

## ORCID

Yang Yang  <https://orcid.org/0000-0001-7439-2156>

## REFERENCES

- Zhang, J., et al.: Bandpass filters using multi-mode square ring resonators. *IET Microw. Antennas Propag.* 12(10), 1656–1665 (2018)
- Bi, X., et al.: A compact sept-band bandpass filter utilising a single multi-mode resonator. *IET Microw. Antennas Propag.* 13(12), 2013–2019 (2019)
- Griol, A., Marti, J., Sempere, L.: Microstrip multistage coupled ring bandpass filters using spur-line filters for harmonic suppression. *IET Electron. Lett.* 37(9), 572–573 (2001)
- Velez, A., et al.: Open complementary split ring resonators (OCSRrs) and their application to wideband CPW band pass filters. *IEEE Microw. Wirel. Comp. Lett.* 19(4), 197–199 (2009)
- Gong, K., et al.: Substrate integrated waveguide quasi-Elliptic filters with controllable electric and magnetic mixed coupling. *IEEE Trans. Microw. Theory Technol.* 60(10), 3071–3078 (2012)
- Chen, R.-S., et al.: Wideband bandpass filter using U-slotted substrate integrated waveguide (SIW) cavities. *IEEE Microw. Wirel. Compon. Lett.* 25(1), 31–33 (2015)
- Lin, J.-Y., et al.: Design of miniaturized triplexers via sharing a single triple-mode cavity resonator. *IEEE Trans. Microw. Theory Technol.* 65(10), 3877–3884 (2017)
- Feng, S.-F., et al.: A triple-mode wideband bandpass filter using single rectangular waveguide cavity. *IEEE Microw. Wirel. Compon. Lett.* 27(2), 117–119 (2017)
- Wu, K.-L.: An optimal circular-waveguide dual-mode filter without tuning screws. *IEEE Trans. Microw. Theory Technol.* 47(3), 271–276 (1999)
- Cogollos, S., et al.: A systematic design procedure of classical dual-mode circular waveguide filters using an equivalent distributed model. *IEEE Trans. Microw. Theory Technol.* 60(4), 1006–1017 (2012)
- Chen, F.-C., et al.: Dual-band coaxial cavity bandpass filter with helical feeding structure and mixed coupling. *IEEE Microw. Wirel. Compon. Lett.* 25(1), 31–33 (2015)
- Doumanis, E., Bulja, S., Kozlov, D.: Compact coaxial filters for BTS applications. *IEEE Microw. Wirel. Compon. Lett.* 27(12), 1077–1079 (2017)
- Wong, S.-W., et al.: Triple-mode dielectric resonator diplexer for base station applications. *IEEE Trans. Microw. Theory Technol.* 63(12), 3947–3953 (2015)
- Nocella, V., et al.: Miniaturized dual-band waveguide filter using TM dielectric-loaded dual-mode cavities. *IEEE Microw. Wirel. Compon. Lett.* 26(5), 310–312 (2016)
- Kwok, R.S., Fiedziuszko, S.J.: Dual-mode helical resonators. *IEEE Trans. Microw. Theory Technol.* 48(3), 474–477 (2000)



16. Doumanis, E., Goussetis, G., Kosmopoulos, S.A.: Inline interdigital pseudo-elliptic helical resonator filters. *IEEE Microw. Wirel. Compon. Lett.* 21(8), 400–402 (2011)
17. Psychogiou, D., Peroulis, D.: Tunable VHF miniaturized helical filters. *IEEE Trans. Microw. Theory Technol.* 62(2), 282–289 (2014)
18. Chu, Q.-X., Zhang, Z.-C.: Dual-band helical filters based on nonuniform pitch helical resonators. *IEEE Trans. Microw. Theory Technol.* 65(8), 2886–2892 (2017)
19. Khan, A.A., Mandal, M.K.: Design of planar diplexer with improved isolation using tunable transmission zeros of a dual-mode cavity filter. *IET Microw. Antennas Propag.* 11(11), 1587–1593 (2016)
20. Aitken, J.R., Hong, J.-S., Hao, Z.-C.: Millimetre wave SIW diplexer circuits with relaxed fabrication tolerances. *IET Microw. Antennas Propag.* 11(8), 1133–1138 (2017)
21. Rauscher, C., et al.: A compact ridge-waveguide contiguous-channel frequency multiplexer. *IEEE Trans. Microw. Theory Technol.* 57(3), 647–656 (2009)
22. Shang, X., et al.: Novel multiplexer topologies based on all-resonator structures. *IEEE Trans. Microw. Theory Technol.* 61(11), 3838–3845 (2013)
23. Zhao, P., Wu, K.-L.: An iterative and analytical approach to optimal synthesis of a multiplexer with a star-junction. *IEEE Trans. Microw. Theory Technol.* 62(12), 3362–3369 (2014)
24. Wong, S.-W., et al.: Cavity balanced and unbalanced diplexer based on triple-mode resonator. *IEEE Trans. Ind. Electron.* 67(6), 4969–4979 (2020)
25. Chen, R.-S., et al.: Miniaturized microwave filter using circular spiral resonators in a single metal cavity. In *Proc. IEEE MITT-S Int. Microw. Symp.*, 1347–1350 (June 2019)
26. Chen, R.-S., et al.: Miniaturized full-metal dual-band filter using dual-mode circular spiral resonators. *IEEE Microw. Wirel. Compon. Lett.* 30(6), 573–576 (2020)
27. Cameron, R.J.: General coupling matrix synthesis methods for Chebyshev filtering functions. *IEEE Trans. Microw. Theory Technol.* 47(4), 433–442 (1999)
28. Cameron, R.J.: Advanced coupling matrix synthesis techniques for microwave filters. *IEEE Trans. Microw. Theory Technol.* 51(1), 1–10 (2003)
29. Liao, C.-K., Chang, C.-Y.: Design of microstrip quadruplet filters with source-load coupling. *IEEE Trans. Microw. Theory Technol.* 53(7), 2302–2308 (2005)
30. Cameron, R.J., Kudsia, C.M., Mansour, R.R.: *Microwave Filters for Communication Systems: Fundamentals, Design, and Applications*. Wiley, New York, NY, USA (2007)
31. Hong, J.-S., Lancaster, M.J.: *Microstrip Filters for RF/Microwave Applications*. Wiley, New York (2001)

**How to cite this article:** Chen RS, Zhu L, Wong SW, et al. Miniaturized full-metal bandpass filter and multiplexer using circular spiral resonator. *IET Microw. Antennas Propag.* 2021;15:606–619. <https://doi.org/10.1049/mia2.12085>